Damage Detection and Identification in Composites by Acoustic Emission, Ultrasonic Inspection and Computer Tomography

Michael Scheerer[1(✉)], Zoltan Simon[1], Michael Marischler[1], and Sascha Senck[2]

[1] Aerospace and Advanced Composites GmbH, Wiener Neustadt, Austria
michael.scheerer@aac-research.at
[2] Fakultät für Technik und Umweltwissenschaften, University of Applied Sciences Upper Austria, Wels, Austria

Abstract. During the life of carbon fiber reinforced plastic (CFRP) components both production-induced imperfections such as fiber misalignment or pores and usage induced damages such as delamination caused by e.g. low velocity impacts or matrix and fiber failure may occur. Such imperfection and damages may lead to a reduction in the load bearing capabilities where early failure detection could be essential for the prognostic of future behaviour of the structure. Within this paper, the authors present the latest results on on-line Acoustic Emission monitoring of different pre-damaged composite coupons. Therefore, composite panels with different amounts of porosity and different impact damages were produced. The pre-damaged composite samples were subjected to a number of interrupted specific loads – bending, shear, tensile and tensile fatigue loads – to assess the Acoustic Emission signature in dependence of load and damage status. The damage status was further assessed by periodic computer tomography and ultrasonic inspection to compare the different NDT methods.

Keywords: Acoustic emission · Ultrasound · Computer tomography · Damage identification · Composites

1 Introduction

In order to bring the advantages of fiber reinforced polymers – high specific strength and stiffness – into applications where mass production is essential e.g. specific aircraft parts such as stringers or frames, automated manufacturing techniques have to replace the wide spread manual production. Depending on the part to be manufactured, infusion methods like Resin Transfer Molding (RTM) or Vacuum Infusion (VI) are such automated production techniques. Depending on the complexity of the parts geometry and the type of the dry pre-form, distortions of the preforms in combination with inhomogeneous flow conditions within the mold during the infiltration can arise which may lead to fiber misalignment and the inclusion of pores and dry spots. Beside the

P. Rizzo and A. Milazzo (Eds.): EWSHM 2022, LNCE 270, pp. 883–891, 2023.
https://doi.org/10.1007/978-3-031-07322-9_89

production induced damages, damaging events during operation such as low velocity impacts that may lead to barely visible impact damages in composite structures have to be taken into account in the design of the structure. A number of publications have used the method of Acoustic Emission to analyze different types of damages in composite materials such as transverse matrix cracking, fiber–matrix de-bonding or fiber fracture where especially frequency based parameters were often used to differentiate between the different type of failure modes [1–7]. Within this paper, the authors presented the latest results on on-line Acoustic Emission monitoring and evaluation during static and dynamic loading of different pre-damaged composite coupons where the damage status was further assessed by computer tomography (CT) and ultrasonic inspection (US).

2 Sample Preparation

Two different type of samples were prepared: ILSS and bending samples with defined impact damage and two types of plates (−45/45 and quasi-isotropic laminates) with different porosities as described in detail in the following chapters.

2.1 Samples with Impact

Six quasi-isotropic CFRP samples with 16 woven fabric layers for ILSS testing and six CFRP samples of the same lay-up for bending tests were subjected to impacts with increasing impact energy of 0J, 5J, 6J, 7J, 8J and 9J using a drop tower type INSTRON Dynatup 9250 HV leading to increasing overall impact damage areas.

2.2 Samples with Porosity

Seven different CFRP plates with two different layups [−45/45]4s and [0/90/−45/−45] 2s out of a NCF prepreg were produced using a vacuum infusion process with different flow aids to obtain plates of different porosities as shown in Fig. 1. All plates have been produced on heat-able Al form. A line inlet and a point outlet were used. The supplied vacuum pressure during the infiltration was constant at p_{abs} = 0.4 bar. The following flow aids have been used: slow infiltration speed – no flow aid, medium infiltration speed – a breeder type Diatex PES340 and high infiltration speed – green flow from Airtech. After the infiltration the panels have been cured on the Al plate for typical cure cycles 4h at 70 °C followed by 3h at 90 °C (recommended cure cycle from the supplier). In addition, a VAP infusion process was used to produce reference panels with very low pore contents. In this process a VAP foil was placed on the dry perform and further molded by standard vacuum bag procedure. The infusion length was limited to the thickness of the laminate.

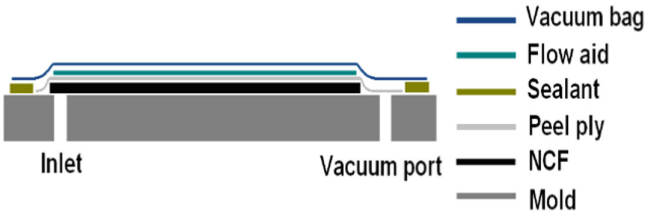

Fig. 1. Schematic view of the vacuum infusion set-up

Table 1. Production parameters of CFRP plates.

Resin	Temperature (infusion, curing, post curing)	Flow aid	Size	Layups	Remark
R&G	40 °C/70 °C/90 °C	**Green** Airtech	250 × 180 mm^2	[−45/45]4s and [0/90/−45/−45]$_{2s}$	Fast flow front
		White Breeder Diatex PES340			Medium flow front
		No			Slow flow front
		VAP		[0/90/−45/−45]$_{2s}$	Through thickness

Table 1 shows the production parameters of the produced CFRP plates. More details about the infusion process can be found in [8].

3 Test Matrix

Table 2 shows performed tests and investigations of the different CFRP samples. After the introduction of the impact damages, the overall damage sizes were determined by US C-scan evaluation. In addition, the crack patterns were visualized by computer tomography (CT). The quality of the produced plates with different porosities were assessed by measurement of the average damping of US wave, image analyses of the CT images and direct measurement of the fiber volume fraction and porosity according to DIN EN 2564. All static and dynamic tests were done with online AE monitoring. Part of the samples (ILSS and dynamic IPS) were tested till failure, whereas all other mechanical tests were stopped before final failure for subsequent NDT investigation by US and CT.

Table 2. Performed tests and investigations of the different CFRP samples.

sample	Defect	Test	NDT
CFRP (50 × 20 × 5.2 mm^3)	Impacts (0, 5, 6, 7, 8, 9J)	ILSS	Online AE/US/CT
CFRP (120 × 20 × 5.2 mm^3)		Bending	
CFRP (180 × 20 × 2 mm^3)	Porosities (low, medium, high)	IPS static	
		IPS dynamic (65 MPa stress/2% strain)	
CFRP (180 × 20 × 2 mm^3)	Porosities (very low, low, medium, high)	Tensile static	
		Tensile dynamic	

4 Experimental Results

4.1 Ultrasonic Inspection and CT Investigation

All US inspections were done with a 4axis automated scanner from Panametrics (now Olympus) using a 10 MHz transducer. For data evaluation C-Scans of the through transmission echo were used. All CT investigations were done with a X-ray micro-computed tomography (XCT) system (Nanotom 180NF, GE phoenix | X-ray) with an isotropic voxel size of 12.5 µm. Voltage was set to 60 kV, current to 260 µA with an exposure time of 900 ms. In total, 1800 projections were recorded. Volume data was reconstructed using filtered back projection applying a beam-hardening correction and an inline median filter using Datos | x (GE phoenix | X-ray) [9, 10]. Figure 2 (left) shows damage area vs impact energy, the US C-scan of impacted ILSS samples and CT images of 8J-impacted samples before and after ILSS testing. Figure 2 (right) shows the average US amplitude and CT predicted porosity vs. measured porosity for the different CFRP plates together with examples of US C-Scans and CT images. The higher the impact energy, the higher was the observed overall damage area of the ILSS samples. The results were similar for the impacted bending samples. A clear delamination growths was observed after ILSS testing as shown in CT images where the original circular shaped delamination from the impact (red) growths over the whole length of the samples (blue). The porosity of the produced plates show an increase in porosity were the porosity increases from plates produced with VAP foil over no flow aid, white flow aid to green flow aid. Continuous US and CT inspections shown no statistically relevant increase in porosity or growths of damages from the pores after static loading. This comes most likely from the limited sensitivity for the detection of small matrix cracks.

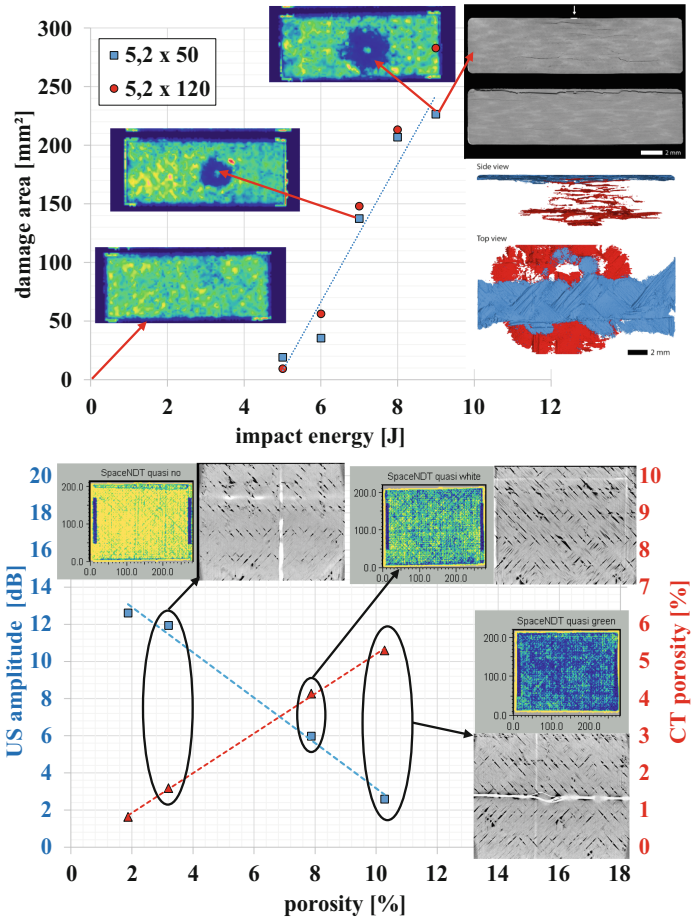

Fig. 2. Top: Damage area vs impact energy, US C-scan of impacted ILSS samples, and CT images of 8J-impacted samples before and after ILSS testing, bottom: average US amplitude and CT predicted porosity vs. measured porosity for the different CFRP plates together with examples of US C-Scans and CT images.

4.2 Acoustic Emission Monitoring

Acoustic emission monitoring was done with an eight channel Mistras DISP system using two broadband AE sensors type WD from Mistras, which were clamped to the top and bottom of the free length of the samples. For data evaluation, the following steps were taken: collection of AE and load data, linear localization of AE events (LE), Filtering of AE data (localized events between the sensors, extraction of the average and peak frequency of the localized events and calculation of the normalized peak frequency (fpn) [5] and presentation of the number of LE as function of the load and normalized peak frequency). Figure 3 shows the AE energy as function of "fpn" of the typical ILSS, bending, in plane shear and tensile tests.

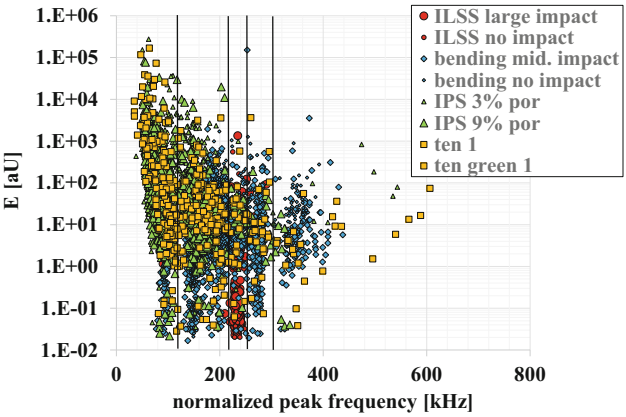

Fig. 3. AE energy as function of "fpn" of the typical ILSS, bending, in plane shear and tensile tests

Five clusters have been identified: f < 120 kHz: Matrix cracking/ 120 kHz < f < 220 kHz: matrix cracking, friction of matrix cracks/220 kHz < f < 250 kHz: interface failure/delamination/250 kHz < f < 300 kHz: delamination friction of delamination fronts/f > 300 kHz: fiber break. Figure 4 shows the AE results of the different static and dynamic loadings: LE as function of shear strain, "fpn" and impact energy of ILSS and bending samples.

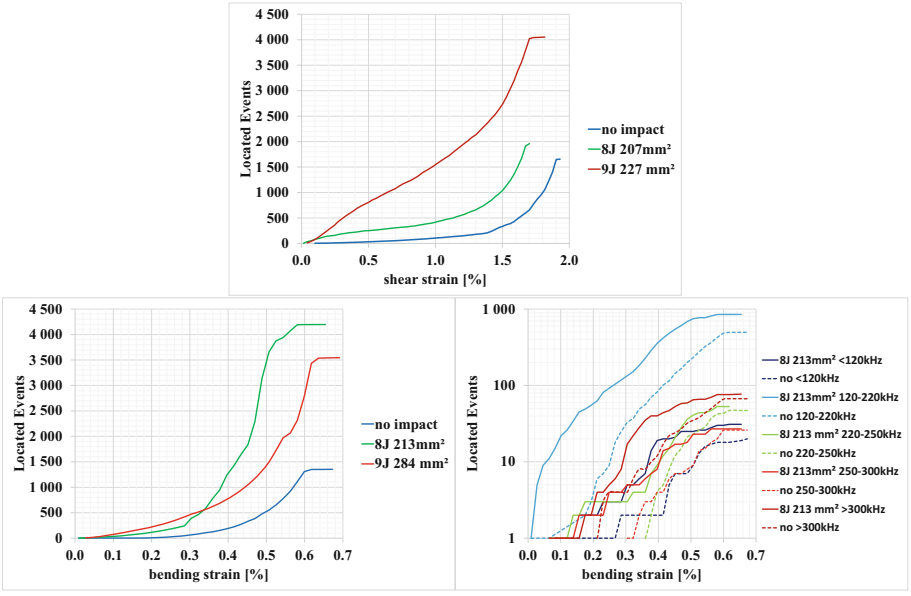

Fig. 4. LE as function of shear strain, average peak frequency and impact energy of ILSS (top) and bending samples (bottom)

For the ILSS and bending samples the number of LE events and slope of the LE vs. strain curve increases with impact size. For the ILSS samples only events with a peak frequency between 220–250 kHz are present, indicating pure delamination damage. For the bending samples the dominant failure mode is matrix cracking and later on fiber failures is indicated by the corresponding frequency ranges. For the impacted samples in addition delamination, starting from the impact induced pre-damage, were observed. Figure 5 shows the LE as function of strain and "fpn" for [−45/45] samples of different porosity and LE as function of stress and "fpn" for [0/90/−45/45] samples of different porosity.

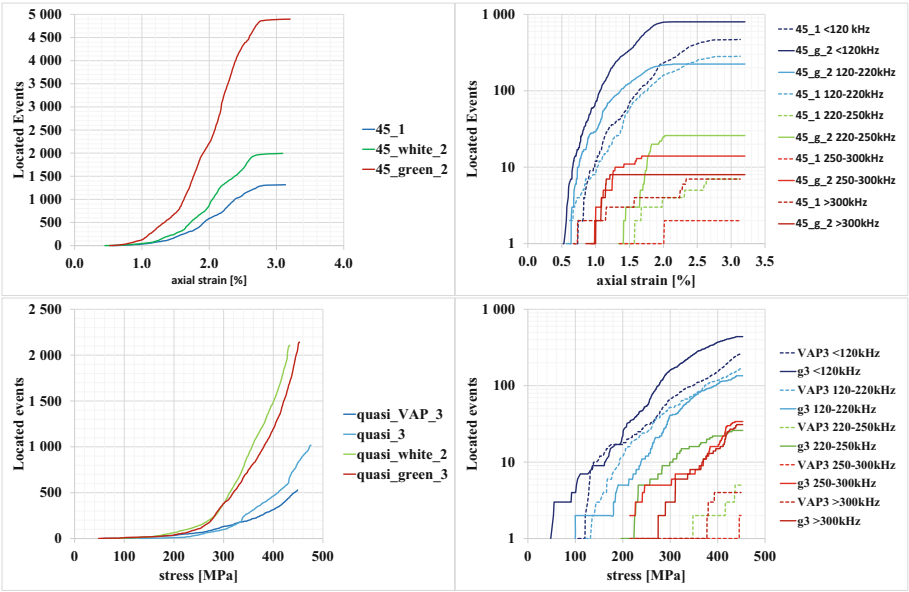

Fig. 5. LE as function of strain and "fpn" for [−45/45] samples of different porosity (top) and LE as function of stress and "fpn" for [0/90/−45/45] samples of different porosity (bottom)

For the static tensile loaded [−45/45] samples (in plane shear test) the number of located events and slope of the LE vs. strain curves increase with the porosity content in the samples. The major contribution is coming from low frequency events indicating dominant matrix failure (<220 kHz) starting at around 0.5% strain. Especially for the samples with higher porosity delamination failure (220–250 kHz) are clearly higher compared to the samples with less porosity. However, the trend is not so strict for the quasi-isotropic samples (higher number of LE event for the sample produced with white flow aid compared to the green flow aid) compared to the trend in the [−45/45] samples. This might be due to the fact, that the pore distribution is not completely homogenous. Also for the quasi-isotropic samples the dominant failure mode is matrix cracking. At load levels higher than 300 MPa delamination and first fiber failures were observed primarily in the samples with higher porosity.

Figure 6 shows the LE as function of load cycles and "fpn" for [−45/45] samples of different porosity in load and strain control.

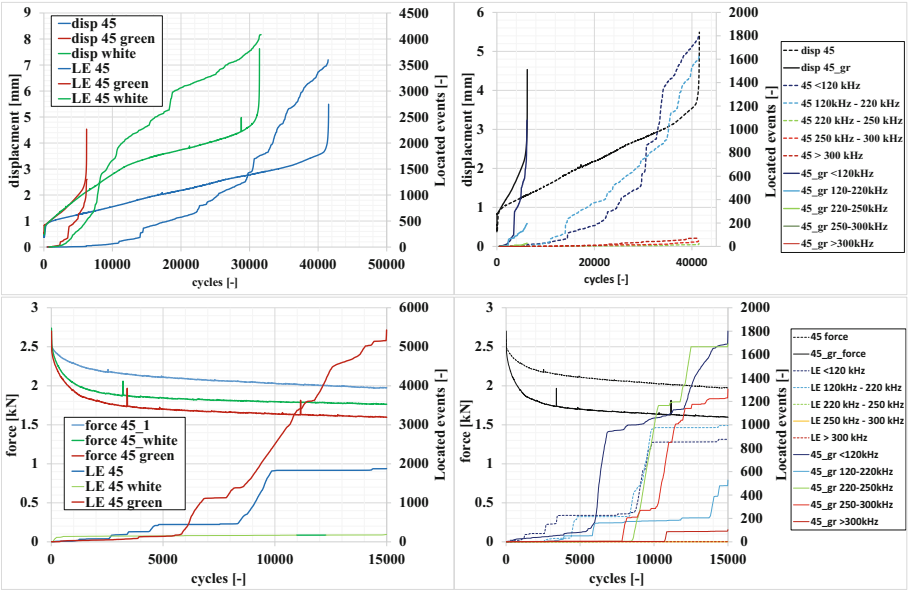

Fig. 6. LE as function of load cycles and "fpn" for [−45/45] samples of different po-rosity in load (top) and strain control (bottom)

The dynamic tensile tests of the [−45/45] samples in load control shows a clear influence of the pore content leading to early failure of the samples with higher porosity indicated also by steeper rise in deflection at constant stress. During this test primarily matrix failure (<220 kHz) occurred. In strain control, the trend is in general similar to the results in stress control. However, the sample produced with white flow aid show rather low AE activity. The major difference between the tests in load control was the strong presence of the dominant presence of events between 220–250 kHz in the sample with the highest porosity (45_gr) indicating mainly delamination starting from the pores as major failure mode up a cycle number of around 8000.

5 Conclusion

CFRP samples of different layups type and sizes of defects – impact damages and porosities – have been subjected to static and dynamic loads with on-line AE monitoring and periodic US and CT investigations. The following conclusion can be drawn:

A clear correlation between average peak frequency and damage mechanism (delamination) were found in ILSS testing. The damage evolution could be verified by US and CT investigations for the growths of impact damages. The higher the amount of

damage (impact or porosity) the higher was the number of LE in ILSS, bending and static and dynamic tensile testing of [−45/45] laminates. Depending on the amount of porosity the damage mechanism my change from primarily matrix failure in static tests to delamination failure in dynamic tests of [−45/45] laminates.

Acknowledgement. The presented work has been funded by the Austrian Promotion Agency within the ASAP projects "SpaceXCT" and "SpaceNDT".

References

1. Boller, C., Chang, F.-K., Fujino, Y.: Encyclopedia of Structural Health Monitoring. Wiley, Hoboken (2009)
2. Sause, M.G.R.: Identification of failure mechanisms in fiber reinforced composites by acoustic emission analysis. In: Proceedings of the 11th International Conference on Structural Safety & Reliability, New York (2013)
3. Ploeckl, M., Sause, M.G.R., Scharinghausen, J., Horn, S.: Failure analysis of NOL-ring specimens by acoustic emission. In: Proceedings of 30th European Conference on Acoustic Emission Testing, Granada, Spain (2012)
4. Sofer, M.G.R., Cienciala, J., Fusek, M., Pavlícek, P., Moravec, R.: Damage analysis of composite CFRP tubes using acoustic emission monitoring and pattern recognition approach. Materials **14**, 786 (2021)
5. Sause, M.G.R., Gribov, A., Unwin, A.R., Horn, S.: Pattern recognition approach to identify natural clusters of acoustic emission signals. Pattern Recogn. Lett. **33**, 17–23 (2012)
6. Godin, N., Reynaud, P., Fantozzi, G.: Challenges and limitations in the identification of acoustic emission signature of damage mechanisms in composites materials. Appl. Sci. **8**, 1267 (2018)
7. Saeedifar, M., Zarouchas, D.: Damage characterization of laminated composites using acoustic emission: a review. Compos. Bart B **195**, 108039 (2020)
8. Scheerer, M., et al.: Effect of production induced porosity on the structural behaviour and damage onset in NCF composites. In: Proceedings of the 15th Conference on Composite Materials, June 2012, Venice, Italy (2012)
9. Senck, S., Planck, B., Kastner, J., Revol, V., Dobes, K., Scheerer, M.: Non-destructive evaluation of defects in polymer matrix composites for aerospace applications using X-ray Talbot-Lau interferometry and micro CT. In: Proceedings of the 58th AIAA, 9–13 January 2017, Texas, USA (2017)
10. Senck, S., et al.: Microcrack characterization in loaded CFRP laminates using quantitative two- and three-dimensional X-ray dark-field imaging. Compos. Part A **115**, 206–214 (2018)